JGR Biogeosciences

RESEARCH ARTICLE
10.1029/2019JG005331

Key Point:
- Climatological indices from hydrologic model used to describe variability in conifers early and latewood rings

Correspondence to:
E. Shamir,
eshamir@hrcwater.org

Citation:
Shamir, E., Meko, D., Touchan, R., Lepley, K. S., Campbell, R., Kaliff, R. N., & Georgakakos, K. P. (2020). Snowpack- and soil water content-related hydrologic indices and their association with radial growth of conifers in the Sierra Nevada, California. *Journal of Geophysical Research: Biogeosciences*, *125*, e2019JG005331. https://doi.org/10.1029/2019JG005331

Received 28 JUN 2019
Accepted 12 DEC 2019
Accepted article online 18 DEC 2019

Snowpack- and Soil Water Content-Related Hydrologic Indices and Their Association With Radial Growth of Conifers in the Sierra Nevada, California

Eylon Shamir[1], Dave Meko[2], Ramzi Touchan[2], Kai S. Lepley[2], Rochelle Campbell[1], Rebecca N. Kaliff[1], and Konstantine P. Georgakakos[1,3]

[1]Hydrologic Research Center, San Diego, CA, USA, [2]Laboratory of Tree-Ring Research, University of Arizona, Tucson, AZ, USA, [3]Scripps Institution of Oceanography, University of California San Diego, La Jolla, CA, USA

Abstract The utility of a high-resolution snow-hydrologic model to derive climatological indices that describe the variability in radial growth of four conifer species in two Sierra Nevada sites is presented herein. Nine annual indices associated with radial growth were developed to represent the winter dormancy, characteristics of the snowpack and soil water content, and the duration of the seasons. Site chronologies of earlywood (EW) and latewood (LW) ring widths were developed for mountain hemlock (*Tsuga mertensiana*), red fir (*Abies magnifica*), white fir (*Abies concolor*), and ponderosa pine (*Pinus ponderosa*) at two sites on leeward and windward slopes. The signal strength for annual climatological indices derived from model output was tested with correlation and regression, in combination with principal components analysis. Results show significant snow-related climate signal in the tree-ring data, with substantial differences between species and between EW and LW. Dependence on previous year's snow and soil moisture (a lagged response) were found for EW of hemlock and red fir. The primary EW-LW signal contrast for those species is a shift toward dependence on current-year moisture conditions for LW, especially for red fir. Lagged climate response was less evident for white fir and ponderosa pine. Regression of tree-ring series on principal components of climatological indices showed a stronger average signal in EW ($R^2 = 0.48$) than in LW ($R^2 = 0.35$). Differences in tree-ring hydrologic signal at the two sites are attributed to microclimate and contrasts in snow regime. Results attest to the hydrologic model usefulness for investigating temporal relationships between tree rings and local climate.

1. Introduction

Tree rings have been widely used to reconstruct hydroclimatic variables in the western United States, including precipitation (e.g., Gray et al., 2004; Meko et al., 2011; Touchan et al., 2011), temperature (e.g., Biondi et al., 1999; Briffa et al., 1992; Graumlich, 1993), streamflow (e.g., Biondi & Meko, 2019; Graham & Hughes, 2007; Graumlich et al., 2003; Woodhouse et al., 2006), snowfall and snow water equivalent (e.g., Anderson, Moser, et al., 2012; Belmecheri et al., 2016; Pederson et al., 2011; Timilsena & Piechota, 2008; Tunnicliff, 1975; Woodhouse, 2003), soil water content (e.g., Anderson, Tootle, et al., 2012; Yin et al., 2008), and drought indices (e.g., Cook et al., 1999, 2007; Meko & Woodhouse, 2005; Stockton & Meko, 1975). These aforementioned hydroclimatic reconstructions were developed at the watershed or regional scales using monthly or temporally coarser observation data sets.

In some regions, tree growth is unmistakably limited by the availability of either energy or water (e.g., Stephenson, 1990), and therefore, a single climatic variable that represents this growth-limiting factor can explain a large portion of the tree radial growth variability.

In our study area, in California's Sierra Nevada, the growth-limiting factor is likely dominated by the seasonal interplay between energy and water that determines the timing, duration, and quantity of water available for the trees during their growing season (e.g., Graumlich & Brubaker, 1986; Nakawatase & Peterson, 2006; Vaganov et al., 1999). This interplay is expressed by the interaction between the seasonal snowpack and the soil column, which in the Sierra Nevada is highly variable in space and time (e.g., Harpold, 2016).

The annual phenological cycle of high-elevation conifers in the Mediterranean climate of the Sierra Nevada broadly has three stages. First is restricted growth or complete photosynthetic dormancy during the cold

winter months (~November–May) due to the short photoperiod and low temperature. Second is optimal growth during the spring when warm temperature and soil water from melted snow is available for transpiration (~April–July). Third is slowdown and limited growth during the summer to early-fall period of high temperature, little rain, large vapor pressure deficit, and depleted soil water content in areas with limited soil water storage (~August–October; e.g., Stephenson, 1990). Tree species differ in their tolerance during the limited growth seasons (winter or summer) and in their growth rate during the growing season (e.g., Kelly & Goulden, 2016; Royce & Barbour, 2001). Moreover, the large climatic interannual variability and the terrain-driven spatial variability of temperature and rain-snow mixture translate to large spatiotemporal variability in the duration of these phenological stages (e.g., Bunn et al., 2018; Royce & Barbour, 2001).

Inferences that tree-ring growth variability is controlled by growing season properties are often implicit and based on cross-correlation of tree-ring series with multimonthly means of climatic variables such as precipitation, temperature, and snow (e.g., Littel et al., 2008; Peterson & Peterson, 2001). Our objective is to explore the use of tailored annual climate indices that explicitly represent the important seasonal factors that explain tree growth variability. Since congruent space-time soil and snow observations are rarely available, we rely on output from hydrologic modeling to describe these climatic indices and their spatial and temporal variability. We evaluate this methodology using four conifer species—mountain hemlock (*Tsuga mertensiana)*, red fir (*Abies magnifica*), white fir (*Abies concolor*), and ponderosa pine (*Pinus ponderosa*) from two sites that are hydroclimatically different despite their close proximity (less than 20 km apart).

In conifers, earlywood (EW) develops early in the growing season and consists of layers of relatively large, thin-walled cells. Latewood develops later and consists of layers of narrower, denser cells with thicker walls (e.g., Fritts, 1976). The anatomical and color contrast between latewood and the following year's earlywood is seen in a radial section as a series of concentric tree rings. The relative timing of features within the growing season is recorded by the position of the ring-features in the sequence of cells making up the annual ring. For example, in the southwestern interior United States, the position of a band of increased wood density—false latewood band—in conifers has been used as a marker of a slowdown in cambial growth associated with the dry fore-summer characteristic of the North American Monsoon system; cambial growth following the band has been applied to reconstruct summer precipitation (e.g., Griffin et al., 2013) and temperature (e.g., Briffa et al., 1988).

Our objectives are to improve understanding of snowpack-related climate signals in the four tree species from the sample sites and to illustrate the use of a high-resolution hydrologic model as a dendrohydrological tool. We first describe the development of the tree-ring chronologies and essential components of the hydrologic model, run at a 6-hourly time step, and the annual climatological indices derived from the model output. We then examine the statistical relationship of model output and climatological indices with EW and LW width chronologies from the two study sites.

2. Data and Methods

2.1. Study Area

The two sites in the central Sierra Nevada selected for this study are Carpenter Ridge (CPR; ~2,500 m above mean sea level) and Truckee Ranger Station (TRS; ~1,980 m above mean sea level). The CPR site is located on the windward slope of the mountains, in the South Yuba River watershed, and the TRS site is located on the leeward slope, in the Truckee River watershed (Figure 1 and Table 1).

The geology at both sites is volcanic, with Quaternary rocks and minor pyroclastic deposits at TRS and Tertiary pyroclastic and volcanic mudflow deposits at CPR. The soil at TRS is about 1 m in depth, and the soil at CPR is shallower than 1 m. Both sites are well drained with sandy loam topsoil. The subsoil is clay loam at CPR and sandy clay loam at TRS.

Most precipitation events, which alternate between rainfall and snowfall, occur in November–April, whereas June–September is generally dry and hot with infrequent convective rainfall events. Seasonal snowpack at high elevations (typically above 1,500 m) develops during November–April and completely ablates during the spring and summer (April–August). Precipitation spatial variability is driven strongly by orographic lifting that leads to enhancement on the windward (western) slopes and reduction on the leeward (eastern) slopes (e.g., Lundquist et al., 2010; Pandey et al., 1999; Wang & Georgakakos, 2005). The soil in

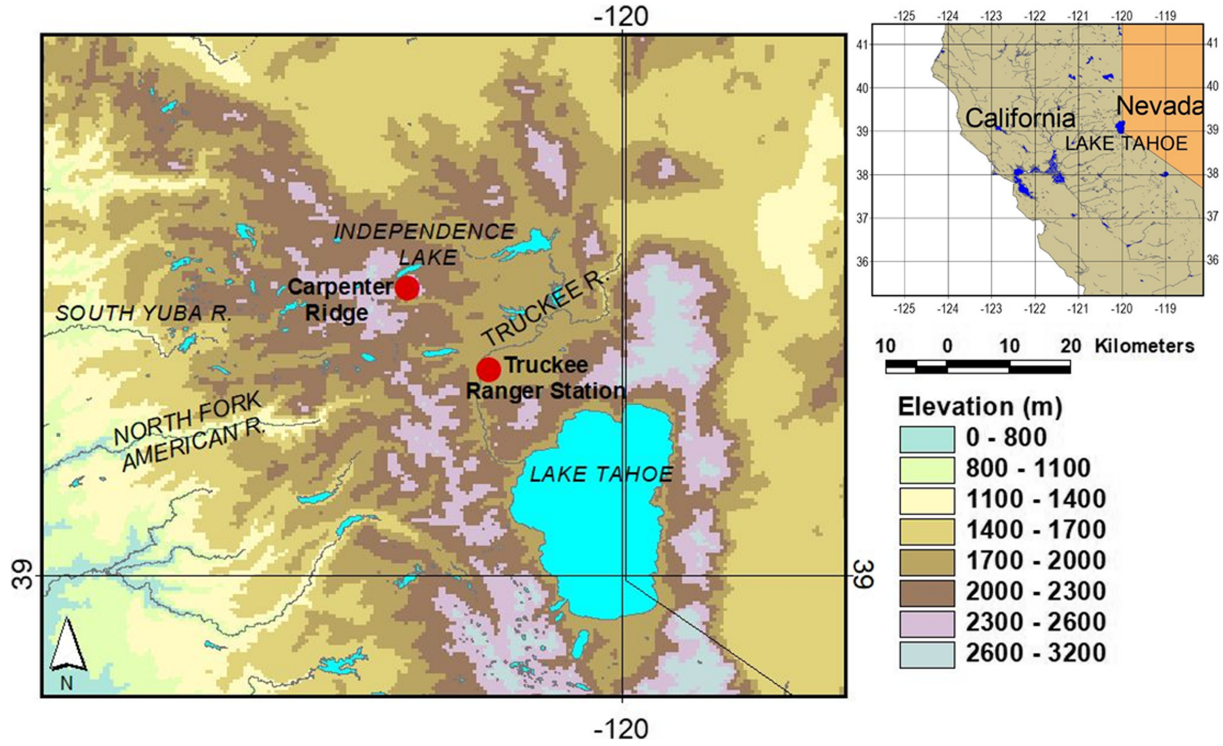

Figure 1. Map of the study region. Tree sites are marked by red dots.

our study area rarely freezes, and the occasional events with soil temperature below 0 °C typically last for only several hours.

2.2. Tree-Ring Chronologies

Field collection in the summers of 2015 and 2016 yielded the four sampled species at the two sites (Table 1). We sampled large and mature trees without noticeable competition for resources from neighboring trees. Ring-width variability in such trees is likely due mainly to climate. Moreover, we selected trees on sloping terrain, not near streams, springs, or ponding water, to reduce the chance of roots tapping multiyear water sources. The sampling strategy favors sensitivity of tree growth to interannual climate variability.

Two increment cores were taken at breast height from 20 trees of each species. Samples were surfaced and cross-dated following standard dendrochronological techniques (Stokes & Smiley, 1996). Total ring widths, EW width, and LW width of each core were measured to the nearest 0.01 mm using a VELMEX measurement system (Velmex Inc., 2016) and Tellervo software (Brewer, 2014). Crossdating and measurement accuracy were verified using COFECHA (Grissino-Mayer, 2001; Holmes, 1983). These quality control measures also help eliminate trees whose moisture supply comes from a multiyear storage in bedrock, as ring-width patterns from such trees are likely to have high persistence and to fail tests for high-frequency correlation —as emphasized by COFECHA.

Each tree-ring widths series was fit with a cubic smoothing spline having a frequency response of 0.5 at a wavelength equal to 67% of the series length to remove trend indistinguishable from growth variations

Table 1
Tree-Ring Site Information

Code	Site Name	Elevation (m)	Latitude	Longitude	Species	Common Name
CPRA	Carpenter Ridge (CPR)	2490–2525	39.4172	−120.3121	*Abies magnifica*	California red fir
CPRT	Carpenter Ridge (CPR)	2490–2516	39.4167	−120.3110	*Tsuga mertensiana*	Mountain hemlock
TRSA	Truckee Ranger Station (TRS)	1970–1985	39.2988	−120.1915	*Abies concolor*	White fir
TRSP	Truckee Ranger Station (TRS)	1970–1980	39.2981	−120.1917	*Pinus ponderosa*	Ponderosa pine

associated with tree age, size, and stand dynamics (Cook & Kairiukstis, 1990). The detrended series were then prewhitened with low-order autoregressive models to remove year-to-year persistence expected from biological processes such as food storage and multiyear needle retention. Indices from individual cores were combined into site chronologies for each combination of site and species using a biweight robust estimate of the mean using program ARSTAN (Cook & Holmes, 1999; Cook & Krusic, 2005).

LW chronologies were further modified to "adjusted LW" by linear regression (Meko & Baisan, 2001) to remove statistical dependence of LW width on preceding EW width. LW chronologies used in subsequent analyses here are adjusted LW. The earlywood, latewood, and total ring width data are archived at the International Tree-Ring Data Bank (ITRDB), managed by National Centers for Environmental Information NOAA and the World Data Center for Paleoclimatology. The ITRDB identification numbers for the four species are CA691, CA692, CA693 and CA694 for CPRA, CPRT, TRSA and TRSP, respectively.

2.3. Hydrometeorological Data

We used a hydrologic model to derive soil water content, snow water equivalent (SWE), and actual evapotranspiration estimates at the sites to compare with the tree chronologies. The hydrologic model provides a data set congruent in space and time that can represent differences between the tree sites in lieu of observations. As model input, we used the gridded 1/16° (~6 km) daily data set of precipitation, wind, and maximum temperature (T_{max}) and minimum temperature (T_{min}) assembled by Livneh et al. (2013) for North America (1915–2015). We adjusted the temperature data using the environmental lapse rate (6.5 °C/km) to account for the differences in elevation of the interpolated grid cells and the tree sites. T_{min} was further corrected as a function of elevation using the following regression derived by comparing gridded Livneh data to local station T_{min}.

$$T_{\text{min}\_corrected} = T_{min} + (0.0053 \cdot Elevation(m)) - 7.5(°\text{C}), \text{Elevation} > 1,450\ (\text{m}), \quad (1)$$

The daily temperature was disaggregated to 6-hr time steps, the required time interval for the hydrologic model input, by setting forth the following assumptions: T_{min} occurs at sunrise, T_{max} occurs at solar noon, and average temperature occurs at sunset. Temperatures vary linearly between these diurnal markers. Using monthly local times for sunset, sunrise, and solar noon for the American River (rounded to the closest hour), hourly temperature estimates were derived and averaged to derive 6-hourly temperature at 3:00, 9:00, 15:00, and 21:00 Pacific Standard Time.

Daily precipitation was evenly disaggregated to 6-hr intervals, and 6-hr wind speed was set at the daily values. For days with missing wind data, we assigned climatological means at the Blue Canyon meteorological station (39.26°N, 120.71°W; 1,510 m) for 3:00, 9:00, 15:00, and 21:00 local time. Blue Canyon relative humidity was also assumed to be representative of the study area. Missing values of relative humidity were replaced with the long-term monthly means at Blue Canyon. Relative humidity was set to 100% during precipitation events.

Observations of soil water content (SWC) and SWE are available from National Resources Conservation Service U.S. Department of Agriculture (http://www.wcc.nrcs.usda.gov/) for Carpenter Ridge (Independence Lake station, ID-541, 39.43°N, −120.31°E, and 2,530 m) and for Truckee (Truckee#2 station, ID-834, 39.3°N, −120.18°E, and 1,972 m). These records were compared with the hydrologic model simulations to tune the model's parameters and evaluate its performance. Soil water content starting in 2004 is available from measurements at 5, 20, and 50 cm below the surface. These measurements are based on soil dielectric permittivity (Stevens Hydra probe I and II, Stevens Water Monitoring Systems, Inc.) with a standard calibration for all soil types. The soil water content measurements are reported as water volumetric fraction (percent). Observed 1980–2014 daily SWE from snow pillows—devices that measure pressure due to overlying snow mass—are also available for Independence Lake and Truckee #2.

2.4. Hydrologic Model

SWC was estimated using the Sacramento Soil Moisture Accounting (SAC-SMA) model, whose structure and parameters are described in Burnash et al. (1973). The model is forced by snowmelt, precipitation, and reference potential evapotranspiration to simulate soil water content and actual evapotranspiration. The SAC-SMA model conceptualizes the storage and transport processes in two soil layers. It represents

the hydrologically active zone of the soil as a relatively thin upper layer (~0.2 m) and a thicker lower layer (~up to 1.5 m). Each layer consists of a tension and a free water reservoir. The free water reservoir represents the water that flows through the interconnected soil pores by gravitational forces, whereas the tension water reservoir represents water held by the surface of the soil particles as films and can only be removed by evapotranspiration. Unless specified differently, the simulated fractional soil water content values reported in this study represent the ratio of the simulated total water content to the fully saturated conditions of the upper and lower soil layers.

We assume that the root zone of the trees is contained within a relatively shallow soil layer; this is also the hydrologically active zone represented by the two layers of the SAC-SMA model. Our field strategy of sampling trees located on sloping surfaces away from potential ponding water or areas with deep soil was aimed at avoiding trees that are likely to tap deeper or more permanent moisture sources. The optimal model to simulate the soil water accessed by the roots of trees is an open research question, beyond the scope of this study, and their remains some possibility that roots might access some moisture outside the SAC-SMA soil zones.

A prior parameterization of the SAC-SMA model for the tree sites was conducted using the Soil Survey Geographic Database (SSURGO), developed by the National Cooperative Soil Survey and archived by the National Resources Conservation Service, U.S. Department of Agriculture. SSURGO polygons at the tree sites were identified and soil texture data were obtained for 0–10, 10–25, 25–50, 50–100, 100–150, and deeper than 150 cm. The soil texture was aggregated into the two SAC-SMA soil layers by selecting the dominant texture for 0–25 and 25–150 cm for the upper and lower layers, respectively, dependent on the prescribed soil depth. The derivation of SAC-SMA model parameters using the SSURGO data set is described in Anderson et al. (2006) and Koren et al. (2003).

To simulate the accumulation and ablation of the snowpack we used the SNOW17 model (Anderson, 1976), a single layer conceptual model that requires air temperature and precipitation data as input. Air temperature is used as an index for the energy exchange across the snow-air interface in order to compute snowmelt and distinguish snowfall from rain. The model continuously accounts for the heat storage of the snowpack and the retention, freezing, thawing, and transmission of liquid water through the pack. Once the snowpack has risen to isothermal conditions at 0 °C, during periods with no precipitation, the air temperature is used in conjunction with seasonally varying melt factors to estimate the rate of melt. During rain on snow events, a simplified energy balance approach is used. The model also accounts for water transport through the snow-soil interface. Initial model parameters for the tree sites were adopted from Shamir and Georgakakos (2006, 2007). Possible shade effect, which may influence melt within the study area, was not considered (Lundquist & Flint, 2006).

For potential evapotranspiration, the California Irrigation Management Information Service (CIMIS-Penman) method was used. The CIMIS-Penman procedure applies empirical coefficients for wind speed (Snyder & Pruitt, 1985) to modify the American Society of Civil Engineers standardized reference evaporation equation (Allen et al., 2005). In agricultural practices, potential evapotranspiration for a specific agricultural crop under optimal health and unlimited water supply is adjusted using seasonally varying adjustment factors (crop coefficients) to represent the crop's evapotranspiration (ET) at different growth stages.

We modified the potential evapotranspiration described above using monthly coefficients to represent the phenological stages of conifers, as suggested by NWSRFS (1999) and Georgakakos and Smith (2001) (conifers' phenological coefficients January–December: 0.5, 0.6, 0.8, 1, 1, 1, 1, 1, 0.8, 0.7, 0.6, and 0.5). The actual evapotranspiration is calculated as a function of potential evapotranspiration and the available soil water content estimated by the SAC-SMA model. In the SAC-SMA model, actual evapotranspiration is first withdrawn from the tension reservoir of the upper layer in a rate that is proportional to the fraction of water content in the upper tension reservoir. The unmet evaporative demand is then withdrawn from the lower tension reservoir at a rate of the fraction water content of the lower tension water to the total soil water tension capacity. Available free water proportionally resupplies the tension reservoirs.

When actual evapotranspiration is equal to potential evapotranspiration, both moisture and energy are available for transpiration and conditions are optimal for tree growth. Deviation from these optimal growth conditions can be measured by the evapotranspiration deficit, which is calculated as the difference of potential and actual evapotranspiration.

Table 2
Definition of Seasonal Onsets

Seasonal onsets (number of days since 1 October)	
Cooling onset	The day that cumulative negative average daily temperature is below −50 °C and continues to decline for at least six consecutive days
Warming onset	Following the day of cooling onset, the day when the cumulative positive average daily temperature exceeds 50 °C and keeps warming for at least six consecutive days
SWE accumulation onset	The first day that SWE is greater than 50 mm for at least 14 consecutive days
SWE melt onset	Following the SWE accumulation onset, the first day that SWE has declined for at least 14 consecutive days
SWE depletion onset	Following the melt onset the first day that SWE is lower than 20 mm for at least 14 consecutive days
SWC wetting onset	The first day that the SWC is above 0.2 for at least six consecutive days
SWC drying onset	The first day following the SWE depletion onset that the SWC is below 0.1 for six consecutive days

2.5. Annual Climatological Indices

Using the 6-hr hydrologic model simulations, we derived nine indices for each water year (1 October–30 September) and for each site to be compared with the annual EW and LW chronologies. The definitions of the seasonal onsets required for the calculation of the indices are presented in Table 2 and Figure 2, and the definitions of the selected indices are shown in Table 3. The indices were selected to represent processes that are likely to strongly influence the interannual variability of the three stages of tree-ring phenology from a climatic perspective.

From the air surface temperature records, we derived indices of the duration of the cold season and the cumulative cooling during the winter. The former represents the period of dormancy (or partial dormancy) of trees, and the latter represents the coldness of the winter season. The cold winters in the high elevations of

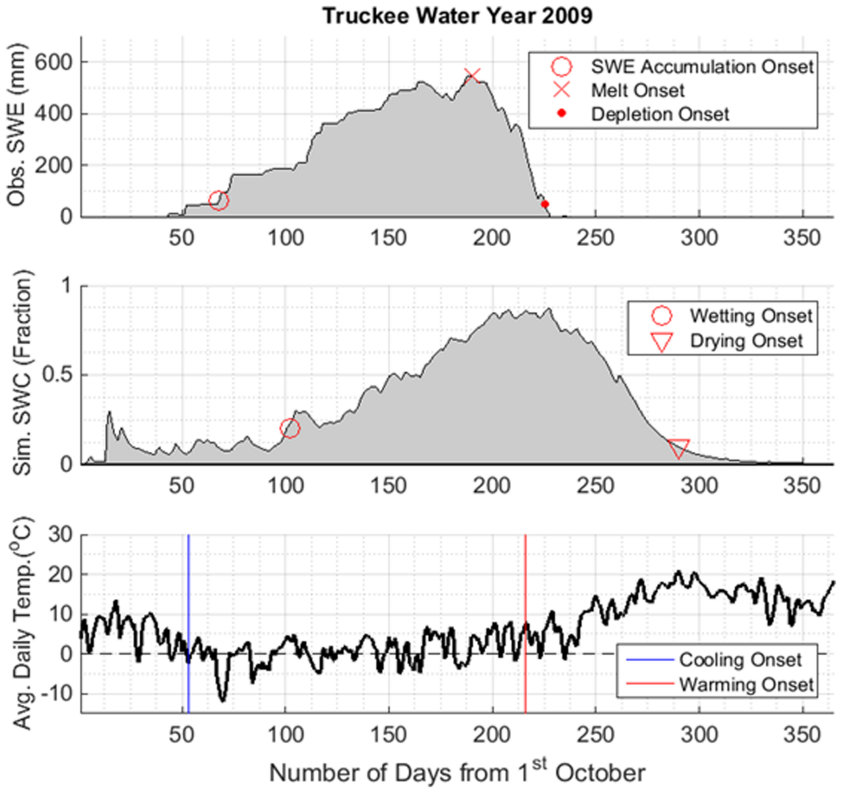

Figure 2. A schematic example for the Truckee site showing the timing of the different onsets described in Table 2.

Table 3
Summary of Annual Climatological Indices Derived From Hydrologic Model Output

Abbreviation	Short definition	Units	Notes
CumCool	Cumulative cooling	°C	Cumulative negative temperature during the cold season
TotSWE	Total SWE	mm	The total accumulated melt over the water year, where SWE is "snow water equivalent"
SnowDur	Snowpack duration	days	Interval from SWE depletion onset to SWE accumulation onset
MeltDur	Melt duration	days	The interval SWE depletion onset to SWE melt onset
MaxSWC	Maximum SWC	fraction	The highest soil water content (SWC)
SWCgt80	Near-saturation duration	days	SWC greater than 80%. Represents days with high SWC during the near-saturation duration, which is the WetDur defined below
WetDur	Wet duration	days	SWC drying onset − SWC wetting onset
DryDur	Dry duration	days	The duration of the dry soil in the summer: SWC wetting onset of the following year − drying onset of the current year
ETdef	Evapotranspiration deficit	mm	Cumulative ET deficit (PET-AET) during the near-saturation duration as defined by the Wet Duration Index (WetDur)

Note. Under "Notes," for duration series, the minus sign refers to a difference in day numbers, with the ending event before the sign and the starting event before the marker (e.g., SWC wetting onset precedes SWC drying onset in the definition of wet duration).

the Sierra Nevada induce periods of limited growth by photosynthetic dormancy with different trees species responding differently to low temperatures and freezing conditions (e.g., Kelly & Goulden, 2016; Royce & Barbour, 2001; Stephenson, 1990).

To derive the cumulative cooling index, it was necessary to identify the beginning and end of the winter in terms of cooling and warming onsets. The cooling onset was estimated as the first day the following two criteria are met: (1) the cumulative sum of daily average temperatures below 0 °C since 1 October exceeds −50 °C and (2) daily average temperature below 0 °C has persisted for at least six consecutive days. The warming onset was conversely defined by adding the days with an average daily temperature that are greater than 0 °C since the day of the cooling onset and searching for the day in which the cumulative positive temperature exceeded 50 °C and a daily average temperature above 0 °C has persisted for at least six days.

The next set of indices is based on the simulated SWE time series. The total SWE during the water year is calculated as the total simulated water-year melt, or total snow-water equivalent (TotSWE). The other two SWE indices represent the duration of the snowpack (SnowDur) and the duration of the melt period (MeltDur). To estimate these durations we define the timing of the SWE accumulation onset, melting onset, and snowpack depletion. SWE accumulation onset is assigned as the first day in which SWE exceeds 50 mm for at least 14 consecutive days. The melt onset is assigned as the first day following the onset of SWE accumulation that SWE declines for at least 14 consecutive days. The SWE depletion day is assigned as the first day following the melt onset with SWE lower than 20 mm for at least 14 consecutive days.

Another set of indices is derived from the simulated soil water content time series. In the Sierra Nevada, the relatively long and often dry summers deplete the soil water content available for transpiration. Transpiration and photosynthesis processes can sometimes be sustained during the dry summer by roots tapping into multiyear water storage in the deep soil and weathered bedrock (Bales et al., 2011, 2018; Klos et al., 2018). Trees that tap into such multiyear water storage will likely to express low interannual variability in their ring widths, and so be excluded from the subset of trees used for the development of site chronologies.

The first soil-based index is the maximum soil water content (MaxSWC). The length of the period of abundant soil moisture for uptake by trees is calculated as the number of days that soil water content exceeds 80% of the storage capacity during the wet duration (near-saturation duration, or SWCgt80). We also selected as indices the duration of the available soil water for the trees (wet duration (WetDur)) and the duration of the dry season (DryDur). The soil water content wetting onset is identified as the first day after 1 October with fractional soil water content higher than 0.2 for at least six consecutive days. The soil water content drying onset is identified as the first day following the depletion of the SWE that the soil water content is below 0.1 for at least six consecutive days. The wet duration is the period between the soil water content wetting and the drying onsets. The dry duration is estimated as the time from the soil water content dry onset to the soil water content wetting onset of the following year. This index represents the duration of the summer water

stress from the perspective of the water content in the soil. It is expected that for drought-sensitive trees a short dry duration implies a relatively moist summer.

The last index, evapotranspiration deficit (ETdef), is the difference of potential evapotranspiration and actual evapotranspiration during the near-saturation duration and represents the inability of the soil water to meet the evaporative demand. If actual evaporation meets demand (zero evapotranspiration deficit), trees are assumed to have optimal growth conditions from water and energy perspectives. While actual evapotranspiration reflects the biologically usable energy and water, the accrued evapotranspiration deficit indicates climatic stress to the trees due to unmet evaporative demand (e.g., Stephenson, 1998).

The climatological indices just described are based on subjective criteria and were developed by exhaustive experimentation with various definitions to represent the seasonal transitions. The goal was to identify robust indices that are sufficiently sensitive to describe the spatial and temporal variability of hydroclimate in the study area. In this study region, the variation of SWE, soil water content, and temperature are seasonal with low year-to-year (interannual) dependency because of long summers that completely deplete the snowpack and dry the soil. Therefore, although the concept may be applicable to other regions, the formulation and definition of the indices should be tailored to the region of interest.

2.6. Assessment of Tree-Ring Hydroclimatic Signal

The strength of the hydroclimatic signal in the EW and LW chronologies was assessed by correlation analysis, principal component analysis, and multiple linear regression (MLR) using the climatological indices described in the previous section. Significant correlations of EW and LW with climatological indices were color-mapped to identify important relationships. Temporal change in strength of hydrologic signal was assessed by computing correlations for different time segments. To explore possible reasons for observed notable changes in signal strength, we checked for differences in the distributions of time series from one segment of the series to another with an F test (e.g., Haan, 2002).

Regression of EW and LW chronologies on principal components (PCs) of climatological indices was used to assess the percentage of tree-ring (EW and LW) variance that is explained by linear combinations of the highly intercorrelated annual climatological indices. PCs were calculated using a singular value decomposition methodology. General descriptions of statistical methods for principal component analysis and regression can be found in standard statistics texts for the environmental sciences (e.g., Haan, 2002). We guarded against overfitting of regression models by not including additional predictors in the model if they did not lead to increasing adjusted R^2 (Myers, 1990), and by applying leave-one-out cross-validation (Hastie et al., 2013; Michaelsen, 1987) to check performance of models on data not used for calibration. Cross-validation skill was measured by the reduction of error statistic (RE; Fritts et al., 1990).

3. Results and Discussion

3.1. Covariation of Tree-Ring Chronologies

The cross-correlation coefficients of the four EW chronologies indicate a stronger association in EW between species at the same site (0.63 and 0.59 for CPR and TRS, respectively) than between sites (lower than 0.33; Table 4). This demonstrates the effect of microclimate differences between sites on the trees' EW radial growth. The cross-correlation coefficients of the adjusted LW among the four chronologies are much smaller than those for EW, and are statistically insignificant ($\alpha = 0.05$).

EW covariation among the four chronologies is summarized by a time series plot of the four-chronology mean, with coded symbols at large departures from the mean (greater than 1 standard deviation) by individual chronologies (Figure 3a). The four-chronology mean varies considerably on interannual and decadal time scales, with a hint of increased variability in the second half of the 1900–2014 interval. Although the chronologies are highly intercorrelated (Table 4), individual chronologies depart greatly from the mean in some years. A noteworthy departure is a narrow earlywood in red fir at TRS (TRSA) in 1977 (Figure 3a). The winter of 1977 was characterized by record dry conditions across the western United States, associated with a persistent upper level ridge positioned over the west coast (Namias, 1978).

EW departures from the four-chronology mean as a function of sampling site (CPR versus TRS) are summarized in Figure 3b. Although EW variations at the two sites covary strongly, the site-average EW at each site

Table 4
Cross-Correlation Matrix of the Four EW (Left) and LW (Right) Chronologies of the Tree Species

		EW						LW			
		CPRA	CPRT	TRSA	TRSP			CPRA	CPRT	TRSA	TRSP
EW	CPRA		0.63*	0.33*	0.17	LW	CPRA		0.13	0.04	0.17
	CPRT			0.24	0.21		CPRT			0.14	0. 13
	TRSA				0.59*		TRSA				0.21
	TRSP						TRSP				

*Correlation coefficient is significantly different from zero ($\alpha = 0.05$).

departs from the four-chronology average by at least 1 standard deviation in nine years (Figure 3b). Periods of especially large site-specific departures in EW are the droughts of the 1930s and late 1980s to early 1990s. The former is expressed much more strongly at CPR and the latter at TRS.

EW departures of individual species from the site average for CPR (Figure 3c) and TRS (Figure 3d) underscore first of all the strong coherence in growth signal in different species at the same location. Large departures of the species from the site average are infrequent: 3 times—1907, 1916, and 1993—since 1900 at CPR, and only once—1930—at TRS. The three outliers at CPR are all years in which the hemlock had narrow EW

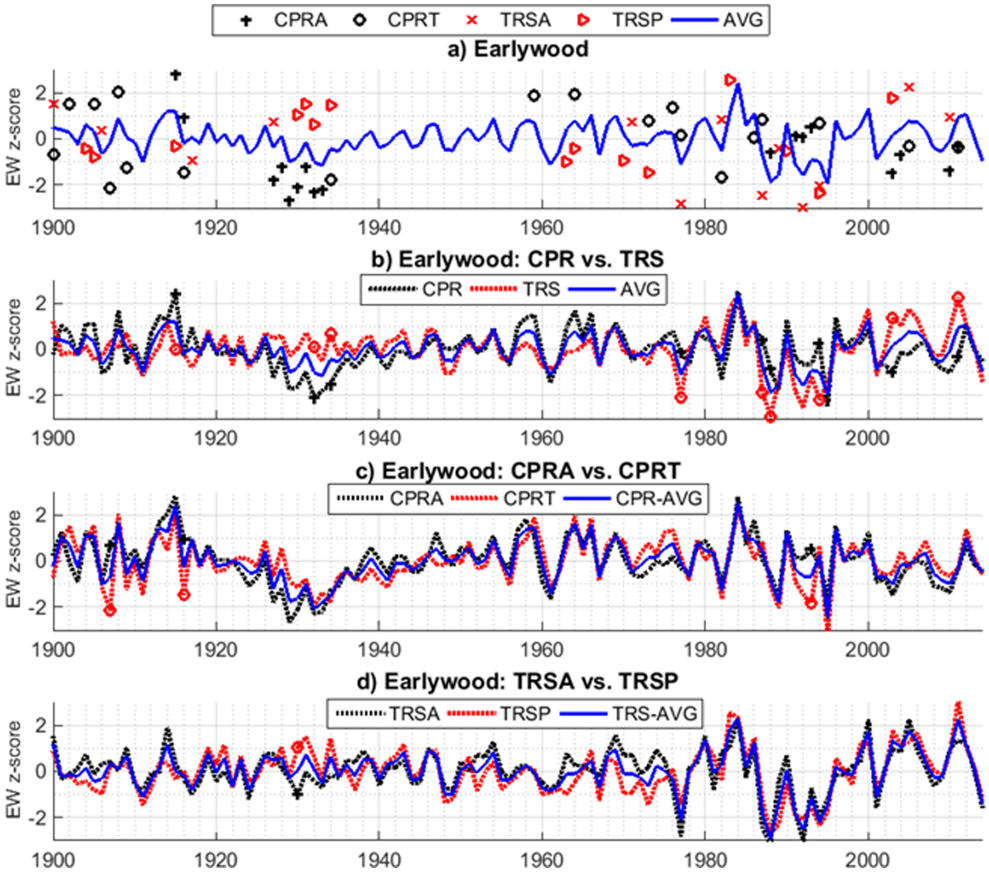

Figure 3. Time series plots summarizing covariation of EW chronologies as a function of species and site, 1900–2014. Series plotted as *z*-scores (zero mean, unit standard deviation) to facilitate comparison. Deviations exceeding 1 standard deviation flagged by coded markers. (a) Average of the four chronologies, representing two sites and two species (blue line). (b) The same four-chronology average (blue line) and individual site averages (CPR and TRS). (c) The average chronology for site CPR and the two species (CPRT and CPRA) chronologies. (d) The average chronology at TRS and two species (TRSA and TRSP) chronologies. See Table 1 for definitions of series ids.

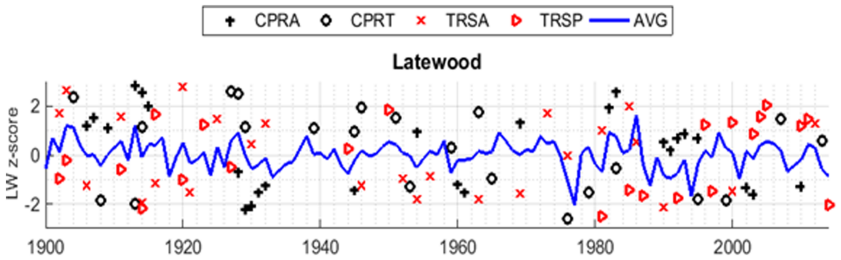

Figure 4. Time series plot of the mean of four LW chronologies, 1900–2014. Series plotted as *z*-scores (zero mean, unit standard deviation). Markers where species chronology differs from the average by more than 1 standard deviation.

and the red fir had wider than normal EW. Species difference in the physiological response to some particular type of climate anomaly is the likely explanation. The aforementioned apparent shift to the higher variance of EW in the second half of the record is consistent across sampling sites and tree species.

LW is much less coherent than EW between species and sites than EW (Figure 4). This lack of coherence is reflected in the low correlations between series (Table 4), which suggests that individual LW series are not sensitive to the same climatological signal. Another contributing factor to the lack of LW coherency could be the larger spatial heterogeneity of the climate signals (e.g., soil water content) in the warm season than in the cool season due to the typical spottiness of convective warm-season precipitation.

3.2. Evaluation of Hydrologic Model

An extensive model evaluation and parameter tuning was carried out by comparing the SWC and SWE model simulations to in situ observations. In the comparison to follow, simulated soil water content is the soil water content fraction integrated over the entire soil column and observed soil water content is the average of the volumetric fraction measured at three depths. Thus, since the soil water content simulations attempt to represent the integrated water content of the entire hydrological active zone of the soil and the observations were taken at three discrete depths, the observed and simulated soil water content may not be expected to represent the same soil water content features. Moreover, the observation stations are installed in forest clearings while the simulations attempt to represent soil water content available to the trees under the forest canopy.

We used the Kling-Gupta efficiency (*KGE*) coefficient as a goodness-of-fit measure to evaluate the model performance (Gupta et al., 2009; Kling et al., 2012).

$$KGE = 1 - \sqrt{(r-1)^2 + (\beta-1)^2 + (\gamma-1)^2} \tag{2}$$

where r is the Pearson correlation coefficient, β is the bias ratio of the averages, and γ is the variability ratio of coefficients of variation of the simulated and observed time series. KGE values can range from $-\infty$ to 1, such that KGE = 1 corresponds to the simulation perfectly matching the observations and KGE > −0.41 indicates that the model performs better than a benchmark of mean SWE or SWC (Knoben et al., 2019). The integration of the correlation, bias, and variability terms in the KGE coefficient provides for a goodness-of-fit measure that, respectively, represents the model's capacity to reproduce the timing, magnitude, and variability of the observed record. Reproducing these properties is a desired skill for a hydrological model.

In Table 5 the KGE values of the SWE (1980–2014 water years) and soil water content (2004–2014 water years) are provided for the daily simulations and the daily anomalies. The daily anomalies were calculated as the daily deviation from the multiyear daily mean. Since SWE and soil water content have a strong seasonal dependence, evaluation for the anomalies provides insight for the model's ability to capture daily changes. Moreover, the evaluation of the anomalies is warranted in cases where the observations and simulations may not measure the exact same property, as the case herein for the soil water content.

The KGE values for the SWE simulations indicate a relatively good skill for both the simulations of the daily values and the anomalies. The KGE values for the soil water content are lower than for the SWE. As the KGE

Table 5
Kling-Gupta Coefficients (KGE) of the Daily Simulations and Anomalies

		Daily simulations	Anomalies
Snow water equivalent (SWE)	Carpenter Ridge	0.86	0.73
	Truckee	0.9	0.68
Soil water content (SWC)	Carpenter Ridge	0.51	0.16
	Truckee	0.24	0.39

Note. Analysis period (water years) is 1980–2014 for SWE and 2004–2014 for SWC.

is an integration of three measures, the timing (r) and variability (γ) terms of the soil water content are comparable to those of the SWE. The reduction in the KGE values is mainly attributed to the increase in the bias ratio (β).

In Figure 5, the daily SWE (top panels) and average daily fractional soil water content of the three sampling depths (bottom panels) are compared with the simulations for October 2009–September 2014. While underestimating the observed SWE at CPR in 2013, the simulated SWE matches the observations well in all other years at both sites. The simulated soil water content (red dashed lines) at CPR and TRS fairly closely tracks observed soil water content (blue solid lines). Simulated soil water content shows an early wetting at both sites in 2013. This discrepancy is likely due to a series of precipitation events being incorrectly assigned as rainfall instead of snowfall by the model. Since the SWE was fairly well simulated in 2014, the soil water content overestimation may be attributed to overestimation of precipitation, underestimation of observed soil water content, or both.

To summarize, despite some discrepancies, the simulations effectively represent the interannual and intraannual variability of SWE and soil water content within a site and the spatial differences between the sites. We reiterate that these are the features that will be compared with the tree indices in the following sections.

3.3. Site Microclimate

Despite their close proximity, sampling sites CPR and TRS have markedly different hydroclimatic regimes, as characterized by model input and output at 6-hr interval for wet water year 1983 and dry water year 2013 (Figure 6).

CPR has a deeper snowpack that lasts about three months longer than the snowpack at TRS (Figure 6). The soil water content at CPR approaches saturation later in the summer when TRS is almost dried up. Compared with TRS, CPR has more precipitation, higher actual evapotranspiration during the summer months, and lower temperature. The higher actual evapotranspiration at CPR during the summer months is because of the higher water availability as reflected by the higher soil water content. It is interesting to point to the interplay between SWE and soil water content at these two sites. The snow lasts longer at CPR and causes soil water content to peak later: in August–September for wet years and in May–June for dry years. Soil water content at CPR slightly decreases during the winter and moisture accumulates during the transition to the spring, while at TRS the soil water content increases at the beginning of the winter. This may be because precipitation events at the beginning of winter appear mostly as snow at high elevation and rainfall at low elevations.

3.4. Tree-Ring Chronologies and Climatological Indices

Exploratory analysis of the correlation between tree-ring variables and climate indices in a sliding 50-year window (not shown) indicated a strengthening of relationships from the first to second halves of the 1915–2014 overlap of data sets. Accordingly, we present the results separately for each half of the record. Cross-correlations between the EW and LW and the nine climatic indices in the year of ring formation and prior year for 1965–2014 are shown in Figure 7 for correlation coefficients significantly different from zero ($\alpha = 0.05$). Corresponding cross-correlations for the 1915–1964 analysis period are shown in Figure 8. A strengthening of drought-related climate signal—particularly with climate of the previous year—in total-width tree-ring indices of red fir and mountain hemlock in the Sierra Nevada from the first to second halves of the twentieth century has been reported by Dolanc et al. (2013). Our findings for EW are consistent

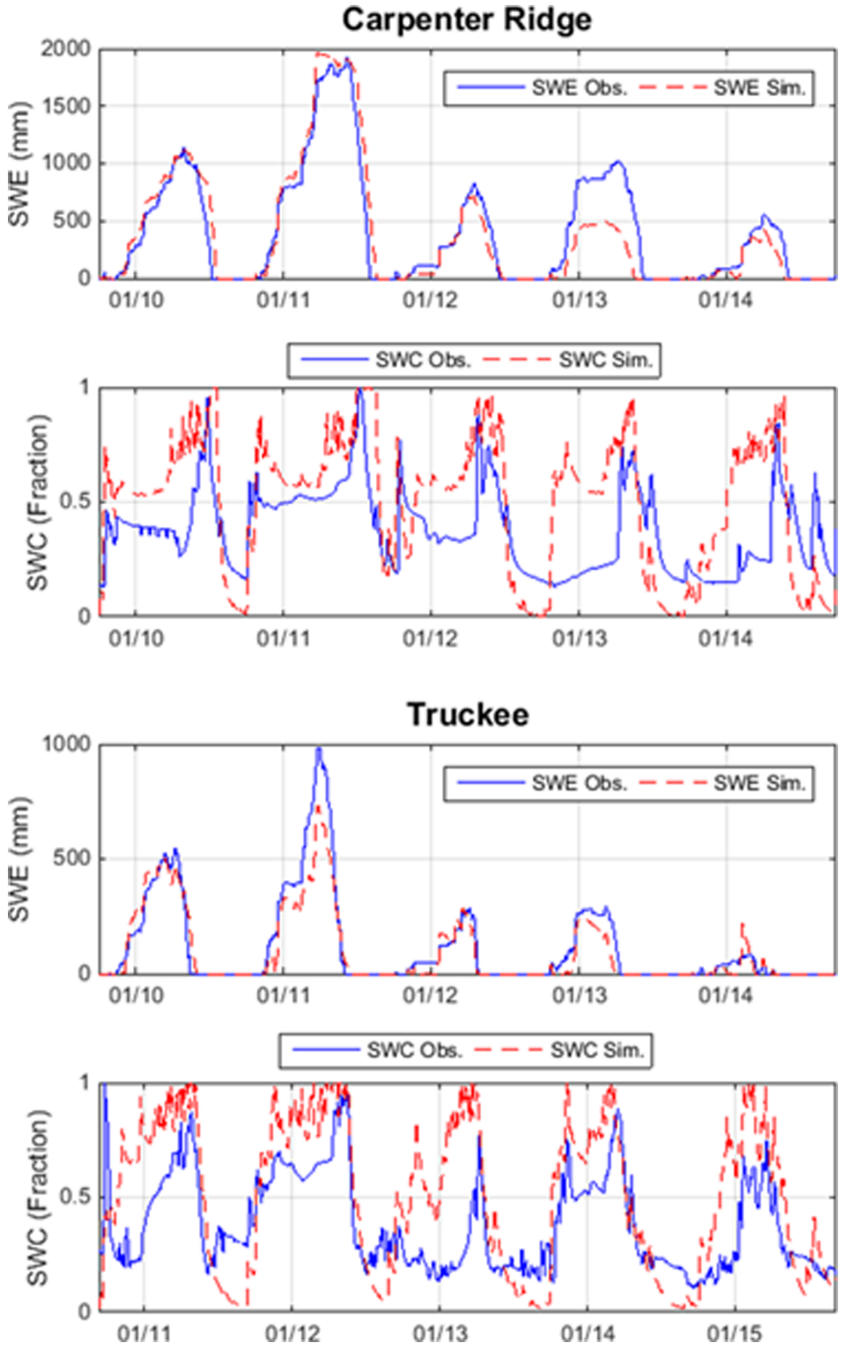

Figure 5. (top panels) Observed (blue solid line) and simulated (red dashed line) daily SWE and (bottom panels) fractional daily soil water content at two tree-ring sites, water years 2010–2014. Simulated soil water content (SWC) of the entire soil column is compared with the average soil moisture measured at depths of 5, 20, and 50 cm deep.

with findings of Dolanc et al. (2013) for total width. The weaker climate correlations in the earlier years may be attributed to either change in the quality of the climatic data or to change in the tree response to climate.

In order to assess whether the differences in correlations between the two periods is associated with changes in the statistical properties of the tree chronologies, a two-sample *F* test was conducted to compare distributions of EW and LW tree chronologies during 1915–1964 and 1965–2014. The null hypothesis of this test is that the chronologies for the two periods are independent samples that belong to the same parent distribution. The test assumes that these samples are normal distributions with equal means and unknown, but equal, variances.

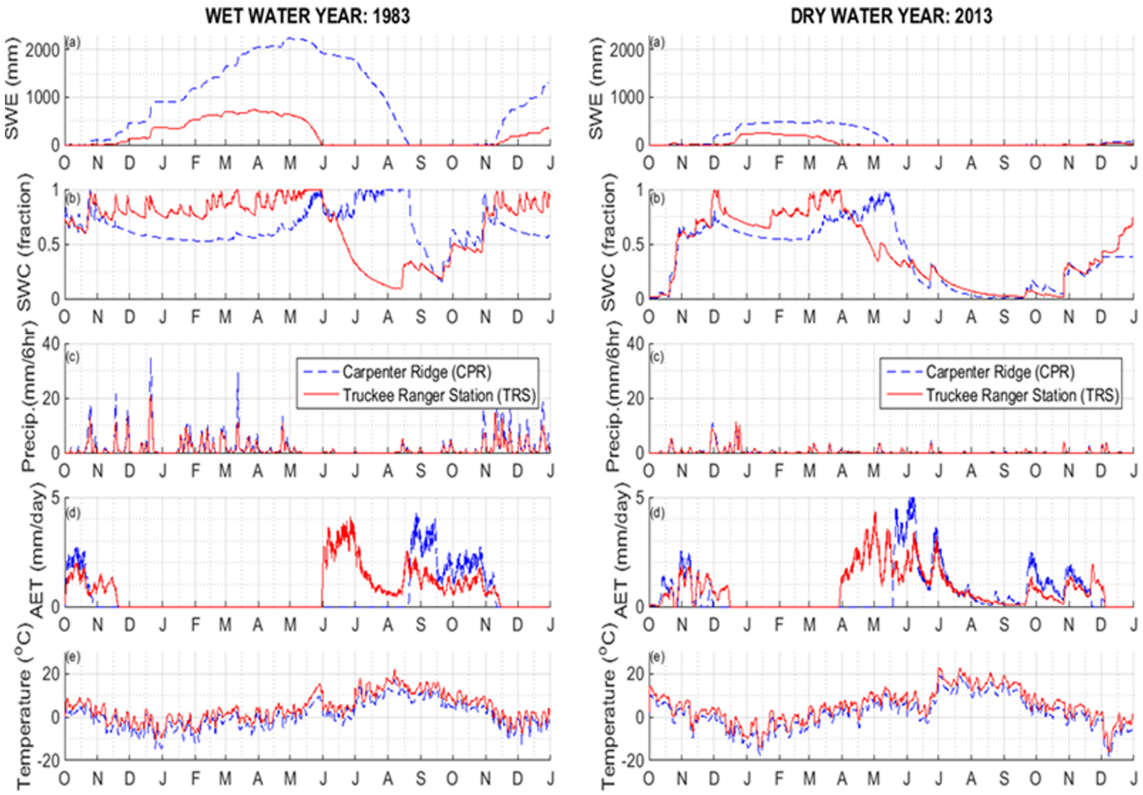

Figure 6. Six-hour resolution climate variation at Carpenter Ridge (blue) and Truckee Ranger Station (red) for wet and dry water years 1983 and 2013, respectively. The variables are (a) simulated snow water equivalent (SWE; mm), (b) simulated soil water content (SWC; fraction), (c) observed precipitation (mm/6 hr), (d) actual evapotranspiration (actual ET; mm/day), and (e) mean daily temperature (°C).

For all chronologies except the LW of red fir and hemlock at CPR, the null hypothesis cannot be rejected ($\alpha = 0.05$). This result implies that no apparent statistical differences are detected in the distributions of the chronologies for the two periods (i.e., 1915–1964 and 1965–2014), and argues for dismissing the observed

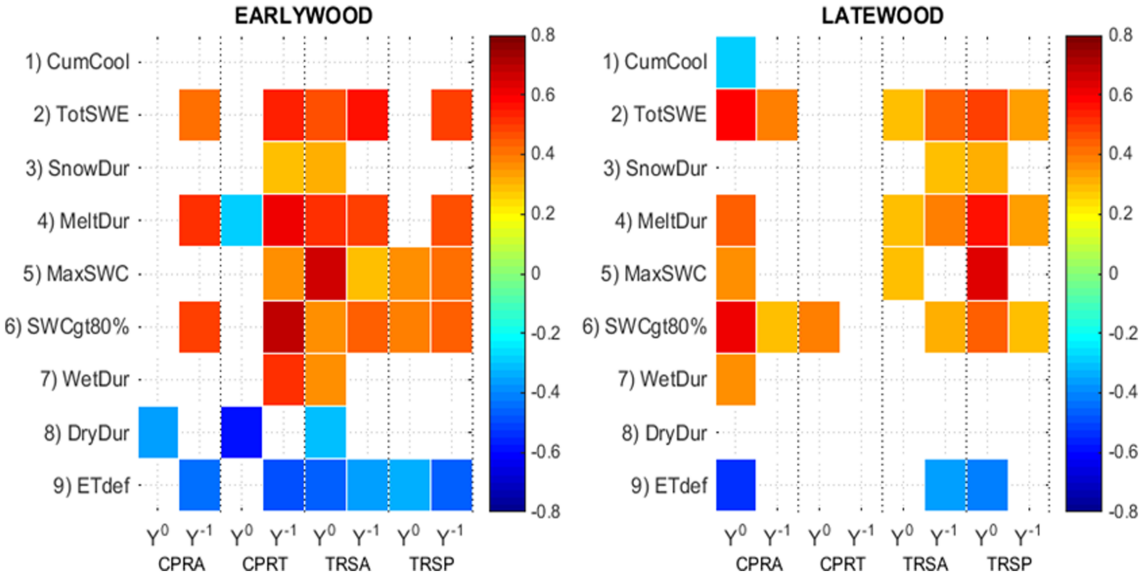

Figure 7. Correlation coefficients between the (left) EW and (right) LW chronologies of the four tree species (1965–2014) and the climatic indices of the current year (Y^0) and previous year (Y^{-1}). The colored boxes indicate correlation coefficient values that are significantly different from zero ($\alpha = 0.05$).

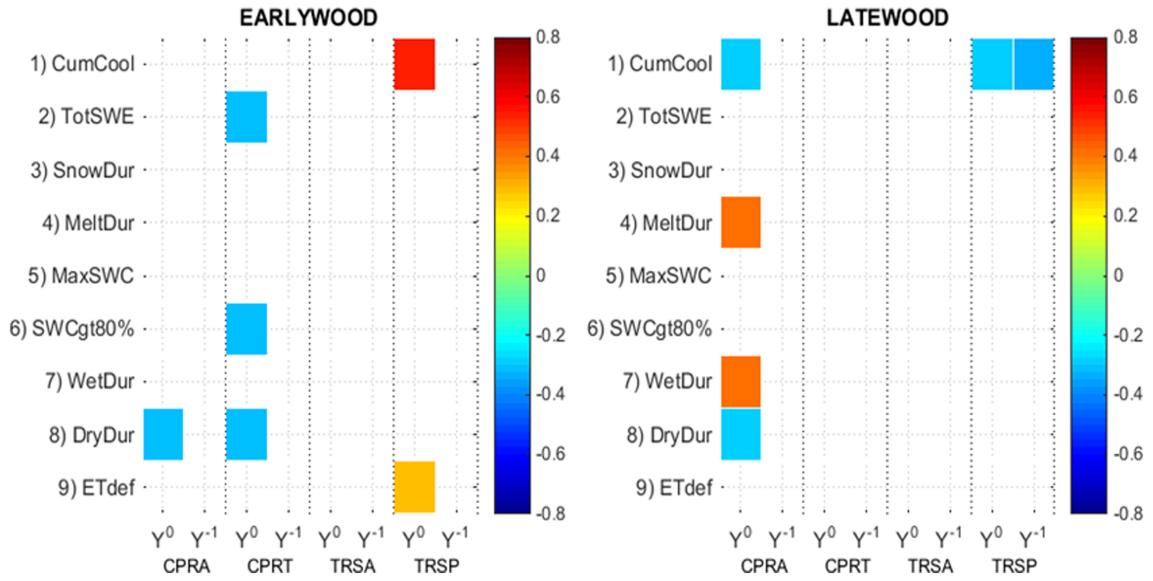

Figure 8. Same as in Figure 6 but for 1915–1964.

increased spread in EW and LW chronologies toward more recent decades (Figures 3 and 4) as an artifact of sampling variability.

A similar *F* test was applied to the CPR and TRS annual total precipitation and average temperature of the time series that were used as input to the hydrologic model. Except from the CPR precipitation, the null hypothesis for all the other annual time series was not rejected, which implies that the two subperiods have the same parent population. However, within 1° × 1° of the study site (39°–40°N, 121°–122°W) the number of gauges available for the interpolation changed sharply over time: about 10 during 1915–1935, gradually increasing during 1935–1955, reaching about 22 for 1955–2000, and gradually decreasing to 15 during 2001–2015. Data from the highest gauge (~2,050 m) was available for only 1915–1918 and 1930–1959, whereas the second highest gauge is 100 m lower. To handle the inconsistency in the data availability, Livneh et al. (2013) in their development of gridded data set selected gauges with at least 20 years of daily records. In addition, the gridded precipitation values were scaled on a monthly basis to match the 1961–1990 and 1981–2010 long-term means of data from the Parameter-Elevation Regressions on Independent Slopes Model (Daly et al., 1994) for 1915–2011 and 2012–2014, respectively. The inconsistency in gauge availability and the scaling that is based on recent climatology can potentially introduce errors and spatial smoothing that reduce the expression of important climatological features, especially in a mountainous environment.

Applying the *F* test to the nine climatological indices at CPR and TRS led to the conclusion that for most indices the samples from the two subperiods come from the same parent population. The exceptions to this conclusion are total SWE, melt duration, maximum soil water content, and near-saturation duration at CPR. The changes in the distribution of these particular indices over time may be attributed to either climatic change or changes in the observational network. Studies have documented strong climate change since 1950 in the central Sierra Nevada in the form of earlier snowmelt, reflected for example in a downward trend in 1 April SWE (e.g., Mote et al., 2005). Our test results did not show any significant change in climatological indices at the TRS site. Perhaps these site-to-site differences in test results reflect some change in the observational network and its representation of the high-elevation climate. A comprehensive investigation of the reason for this change in association strength between the chronologies and the climatological indices is beyond the scope of the manuscript. The climate-signal analysis for the remainder of the manuscript is restricted to the more recent part of the climate record, 1965–2014.

The duration of the cold season was found to have a weak association with the tree indices; the only temperature-based index we selected for further analysis is the cumulative cooling index. EW of both red fir and mountain hemlock at CPR is negatively correlated with current-year dry duration in the 1965–

2014 analysis period (Figure 7). This result implies that a shorter period of drought stress in the summer is associated with wider EW. A negative correlation is also seen for previous-year evapotranspiration deficit and the current-year melt duration in hemlock at CPR. Both species at CPR are positively correlated with the prior year total SWE, MeltDur, near-saturation duration, and wet duration. Hemlock at CPR is also positively correlated with the prior year maximum soil water content. These correlation patterns for EW of the two species at CPR indicate a moisture-limited growth (less moisture, less growth) with a strong lagged dependence on moisture conditions from the previous year.

The strongest EW association with climatological indices is for white fir at TRS (Figure 7; TRSA). White fir EW here is positively correlated with the current-year total SWE, snowpack duration, melt duration, maximum soil water content, near-saturation duration, and wet duration. In addition, it is positively correlated with the previous-year total SWE, melt duration, maximum soil water content, and near-saturation duration. EW at TRSA is also negatively correlated with evapotranspiration deficit during the current and previous years and duration of dry soils in the summer of the current year. These results suggest a drought stress limitation to EW, as the "dry duration" as defined here is the interval of time of dry soil, and high evapotranspiration deficit would tend to be associated with dry soil. The correlation pattern for EW of ponderosa pine at TRS is similar to that of white fir, except that for ponderosa the correlations are stronger with the prior year than with the current year (total SWE, melt duration, maximum soil water content, near-saturation duration, and ETdef). Unlike white fir, ponderosa also has a stronger negative correlation with evapotranspiration deficit of the previous year than with evapotranspiration deficit of the current year.

The strongest LW association with climatological indices is for red fir at CPR (Figure 7; CPRA). Red fir LW is positively correlated with the current-year total SWE, melt duration, maximum soil water content, near-saturation duration, and wet duration, and negatively correlated with cumulative cooling and the dry duration of the current year. In contrast, hemlock at CPR (Figure 7; CPRT) has significant LW correlation with only the current-year available soil moisture (near-saturation duration). At TRS, the strongest association with LW is seen for the TRSP with the current year indices. LW of TRSA is positively correlated with total SWE, melt duration, and maximum soil water content of the current year and total SWE, melt duration, and near-saturation duration of the previous year.

In summary, the EW and LW climate correlations show a striking shift in significant correlation from the previous year for EW to the current year for LW. This shift is most strongly seen for CPRA and TRSP and is a favorable result in suggesting that partial ring measurements may yield separate important information on snow-related climate variable at these sites. Positive response of EW to moisture of the previous year is consistent with total-width studies of red fir and mountain hemlock elsewhere in the Sierra Nevada (Dolanc et al., 2013). The results here also attest to moisture limitation as a primary driving force in EW and LW variation and emphasize that the signal can have a dramatically different manifestation in different species. The strong red fir LW signal for current-year moisture variable is promising for future dendrohydrological studies in the Sierra Nevada, as red fir is widely distributed at high elevations, but has until now not received much attention in climatic reconstruction studies.

3.5. Tree-Ring Variance Explained by Climatological Indices

Regression on PCs of selected climatological indices was used to summarize the strength of the hydroclimatic signal in EW and LW chronologies. This analysis was conducted on the 1965–2014 segment of the time series. Based on the analysis presented above we selected for the principal components analysis five indices (i.e., total SWE, melt duration, maximum soil water content, near-saturation duration, and evapotranspiration deficit) from the year of the ring growth. Separate principal component analyses were run for the CPR and TRS sites, as each has different climatological data.

More than 60% of the variance of the climatological indices is explained by the first PC and more than 85% of the variance is explained by the first three PCs (Figure 9).

The PC loadings of the first three PCs for the two sites weight the importance of the original climatological indices to the PCs. PC1 at both sites is broadly a common moisture signal, with same-sign (negative) loadings on variable positively related to moisture, and an opposite-sign loading on evapotranspiration deficit. Each PC has a corresponding time series, such that a negative value of the time series for PC1, in this case, would correspond to wet conditions at both sites. PC loading patterns for higher-order PCs become increasingly

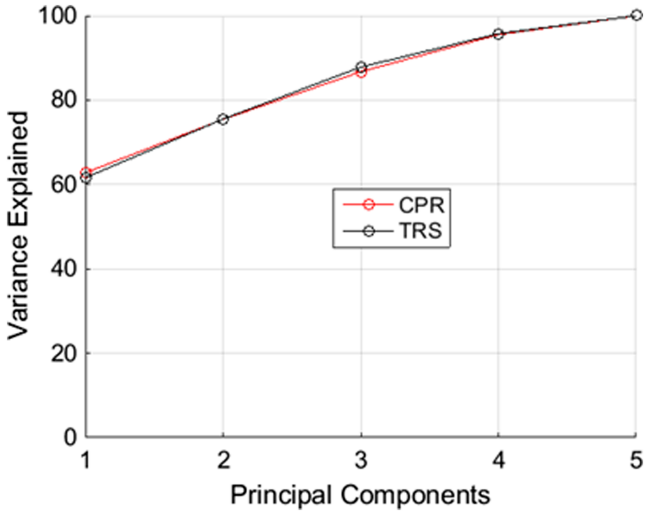

Figure 9. Cumulative variance explained by the principal components of 1965–2014 climatological indices at the two sites.

difficult to interpret because each PC is constrained to be orthogonal to all lower order PCs. Nevertheless, the loadings patterns generally reflect some contrast of above normal values in some indices and below normal in others. For example, PC2 at TRS is a contrast of maximum soil water content and near-saturation duration, which are the soil water content indices (Figure 10). This PC emphasizes years in which the maximum soil water content may be high (low) and yet the duration of the wet interval short (long). PC2 has a different pattern of loadings at the two sites. PC3 is actually quite similar at the two sites, as the signs of loading can be flipped (sign indeterminate) without altering the interpretation: except for SWCgt80%, negative PC3 loadings at CPR correspond to positive loadings at TRS.

Regression (MLR) of each EW and LW chronology on the PCs of the climatological indices at its site yields a regression R^2 that summarizes the strength of the hydroclimatic signal. To allow for the possible lagged influence of climate, we included PCs from the year preceding growth as well as from the year of growth in the regression. MLR was run separately for each of the four EW and LW chronologies using a common analysis period of 1965–2014.

We tested various combinations of predictors from a pool consisting of the first three climate PCs in the year of the tree-ring growth and the preceding year (six potential predictors) in MLR as seen in the following equation:

$$\hat{Y} = a_0 + a_1 PC1_{t-1} + a_2 PC1_{t0} + a_3 PC2_{t-1} + a_4 PC2_{t0} + a_5 PC3_{t-1} + a_6 PC3_{t0} \quad (2)$$

where $\hat{Y}$ is the regression estimate of either EW or LW tree chronologies, a_i are the regression MLR coefficients, the $t-1$ subscript of the PCs indicates the lagged one-year PCs for the climatological indices from the year prior to the ring formation, and subscript $t0$ is for the year of the ring formation.. In estimating these MLR models, predictors were entered sequentially in the order presented in equation (2) until adjusted R^2 failed to increase. The number of predictors selected for the various models for EW and LW ranges from one to six (Table 6; in parenthesis).

Substitution of the PCs of climatological indices into the fitted regression equation yields predicted time series of EW and LW, which are compared with time series of observed EW and LW in Figure 11. Overall, the predicted chronologies track the observed chronologies well, with close synchrony at high and low frequencies for both EW and LW. Only the model for hemlock LW at site CPR (model CPRT) fails to be statistically significant ($\alpha = 0.05$) as measured by the overall F-statistic of regression.

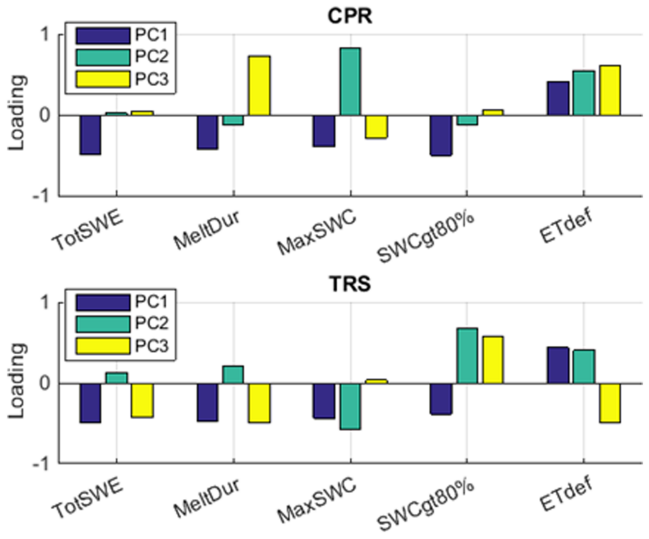

Figure 10. The loadings for the five selected indices of the first three PCs.

The explained variance of EW and LW by the climatological indices averages 42% for all models (Table 6 and Figure 1). Explained variance is highest (58%) for EW at TRSA and lowest (10%) for LW at CPRT. All models show some skill (RE > 0), and models with $R^2 > 0.50$ show only a small drop (0.07–0.13) from R^2 to RE. For comparison in Table 6, we also list (shaded) the corresponding percentage of variance explained in regression of chronologies on total water-year precipitation (P) and average temperature (T) for the year of growth and year preceding growth. These annual P&T values were derived from the time series that were used as input for the hydrologic model. The derivation of the MLR using P&T was conducted exactly as the MLR using the climatological indices as predictors. The same adjusted R^2 method was also used to determine the number of predictors (out of 4) for the MLR on P&T. As previously noted the P&T fluxes are implicitly related to the land surface processes that

Table 6
Percent of the Explained Variance (R^2) of the Four Trees EW and LW Chronologies by MLR, the Number of PC Predictors That Were Used in the MLR (in Parenthesis), and the Reduction of Error Index (RE)

			CPRA	CPRT	TRSA	TRSP	Average
Earlywood width	PC	R^2	0.37 (5)	0.57 (5)	0.58 (4)	0.4 (2)	0.48
		RE	0.23	0.44	0.5	0.36	0.38
	P&T	R^2	0.33 (4)	0.52 (3)	0.4 (2)	0.04 (1)	0.32
		RE	0.21	0.5	0.33	0.03	0.27
Latewood width	PC	R^2	0.56 (4)	0.1 (2)	0.31 (6)	0.43 (2)	0.35
		RE	0.49	0.01	0.15	0.4	0.26
	P&T	R^2	0.63 (4)	0.07 (1)	0.31 (3)	0.28 (1)	0.32
		RE	0.43	0.03	0.09	0.24	0.2

control the trees growth, while the climatological indices are an attempt to explicitly describe the timing of moisture and energy availability that control tree growth. A good performance of the climatological indices in comparison to the P&T suggests that the hydrologic model describes processes that are relevant for the tree growth.

Overall, a larger variance of the chronologies is explained by the climatological indices than the reference MLR using the annual precipitation and temperature, although the single highest R^2 is for the red fir LW model on P&T. The variance explained by the climatic indices is similar to percentages reported in previous studies conducted in the Sierra Nevada looking at summer temperature and winter precipitation (e.g., Bigelow et al., 2014; Dolanc et al., 2013; Sprague, 2009; Yeh & Wensel, 2000).

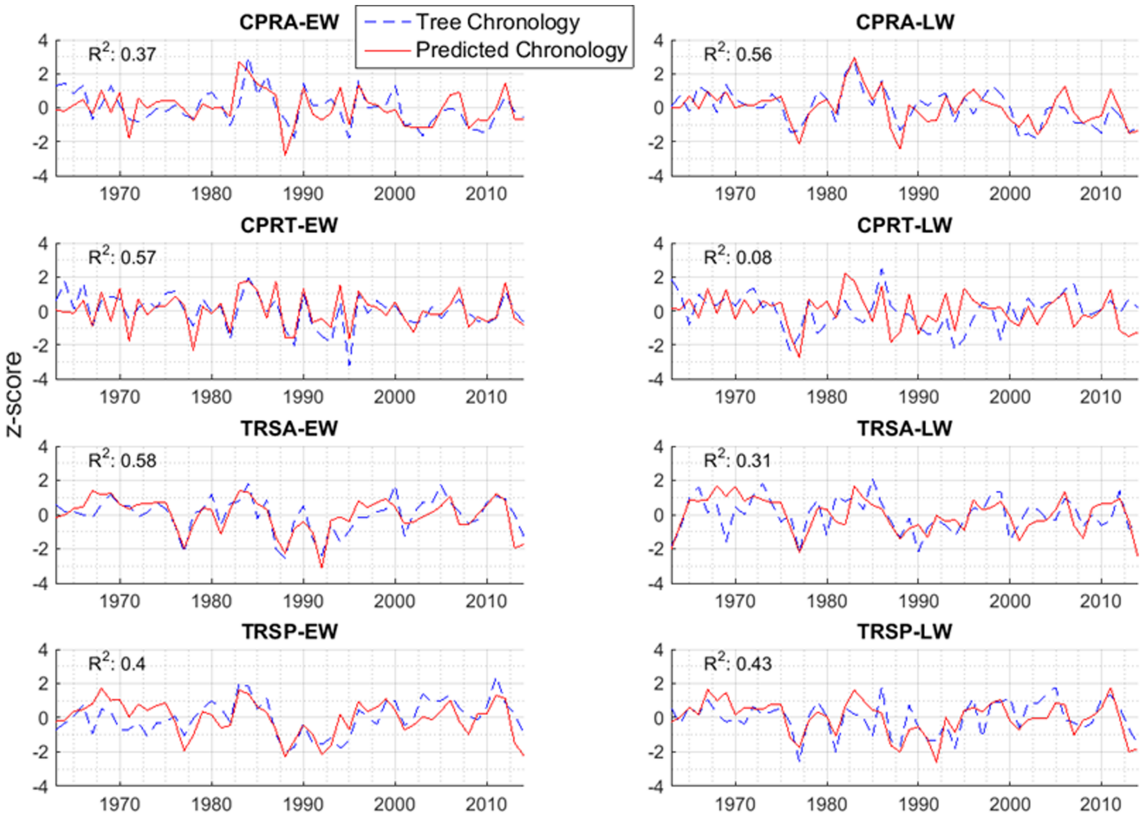

Figure 11. Observed (dashed blue) and predicted (red) standardized (left) EW and (right) LW ring-width chronologies. *R*-squared of the comparison between the chronologies and their estimate are indicated in the top left.

3.6. Uncertainty

The EW and LW variance not explained by the MLR models represents "noise," which includes imperfect specification of the climate inputs and the way in which those inputs are translated to cambial growth. We attempted to minimize the influence of nonclimatic influences such as disturbance and competition for moisture and nutrients by strategic selection of the trees to be sampled. Perfect rendering of climate from tree rings is of course impossible because tree growth responds to some extent to factors other than climate. Some unexplained variance likely stems from the uncertainty associated with both the derivation of the tree chronologies and the climatic description of the sites.

It is possible that signal strength could be increased by including additional trees in the site collections, or by processing the ring widths into site chronologies with different settings for statistical removal of growth trend, etc.

The particular climate indices used in this study necessarily depend on somewhat arbitrary definitions of seasonal offsets (Table 2). Other definitions of offsets would lead to different time series of indices. The selected climatological indices themselves cannot be expected to be optimal for mirroring the way that tree growth might integrate climate inputs over time, as tree phenology would impose its own filter on the climate response. The high-resolution hydrologic model used to derive indices also cannot be expected to exactly reproduce the actual climatological conditions (e.g., soil water content) at the sites. The uncertainty in the hydrologic model simulations is likely stem from the model input, model structure, and model parameters.

An additional source of uncertainty stems from the choice of analysis methods. Regression and correlation by definition measure the strength of linear relationship. Tree radial growth is often controlled by environmental stresses that act as growth thresholds and changes in growth rate may be a nonlinear function of the climatological conditions (Vaganov et al., 2006).

4. Conclusions

We have explored here the use of a high-resolution hydrologic model to identify snowpack- and soil water content-related climatological indices in earlywood and latewood measurements from tree rings of four conifer species at two sites in the central Sierra Nevada of California. These climatological indices aim to explicitly represent the land surface conditions and the timing of the available water and energy that control the tree growth. Precipitation and temperature, the primary input time series to the model, reflect climate variability at the tree-ring sites. The climatological indices proposed here attempt to describe the interaction of meteorological fluxes and the land surface, and to capture the accretion and depletion processes of the snowpack and soil water reservoirs that closely control tree growth.

Annual climatological indices derived from output of the hydrologic model were found to be significantly related to time series of EW and LW indices of the four tree species sampled. Signals for both EW and LW reflect moisture-limited growth. Signal strength and seasonality differ strongly, however, across sites and species and between earlywood and latewood. Earlywood for the sites and species studied most strongly responds positively to hydroclimate of the water year preceding the year of tree-ring growth, and latewood responds mostly to conditions in the current year. This distinction is most strongly expressed in red fir, but also evident in other species. Earlywood width for all four species was correlated with total water-year snowmelt for the water year prior to the ring development. This lag in response is consistent with other recent dendroclimatological studies of total-width chronologies and should be considered in the design of future dendrohydrologic studies to reconstruct snowpack-related variables.

We demonstrated that subannual width measurement (EW and LW) will be beneficial in future application of these tree species to dendrohydologic reconstruction in the Sierra. Multiple linear regression indicates on average 48% and 35% of the variance of earlywood width and latewood width, respectively, can be described by principal components of snowpack-related variables output by the hydrologic model. Important model-output variables include water-year total snowmelt, evapotranspiration deficit, maximum soil moisture, and near-saturation duration that likely represents the growth duration of the trees.

Implications for future research are particularly encouraging for red fir, a species widely distributed in high snowpack areas of the Sierra Nevada, but previously little used in dendrohydrologic reconstruction. Red fir

had not only one of the strongest signals for previous year's soil moisture and snowpack in the earlywood width but also the strongest current year composite moisture signal in the latewood width, where the most important variables were the water-year total snowmelt and the number of days for which soil moisture exceeded 80% of capacity.

The finding of a strengthening of hydroclimatic signal in the earlywood and latewood chronologies from the first to the last halves of the 1915–2014 instrumental period should be addressed for other tree-ring sites and with other basic climatological data. Despite the negative results of our difference-of-distribution *F* test, time series plots suggest increased variability of earlywood and latewood chronologies in the second half of the instrumental record, and previous studies have documented sharp trends in snowmelt regimes in the region since the middle of the twentieth century (e.g., Mote et al., 2005). Earlier snowmelt lower snowpack could favor the strengthening of the tree-ring response to moisture variables as the site becomes more moisture limiting to growth in the summer months.

Finally, this study illustrates the potential of high-resolution hydrologic modeling for identifying linkages of hydrologic variables and processes to tree growth. The modeling approach is more complicated than the simple correlation of tree-ring series with meteorological variables precipitation and temperature. The hydroclimatic series provided by the high-resolution model (e.g., SWE or soil water content at submonthly resolution) are more closely tied conceptually than precipitation and temperature to the moisture conditions sensed by the tree. Follow-up studies could explore the linkage of hydrologic models and mechanistic tree-growth models to better characterize hydroclimatic impacts on tree growth. Such integration will likely enable further exploration of the importance of spatial variability of the climatic variables and enable the development of climatological proxies at finer temporal and spatial scales.

Acknowledgments
This research was funded by the U.S. National Science Foundation (NSF), award 1445889 with supplemental fund from the NSF-Research Experiences for Undergraduates (REU). The NSF-REU provided support for Rebecca Kaliff, who is an undergraduate student at the University of California Berkley for a summer internship at the Hydrologic Research Center, San Diego. The tree-ring earlywood, latewood, and total ring width data of the two study sites were archived at the International Tree-Ring Data Bank (ITRDB), managed by National Centers for Environmental Information NOAA and the World Data Center for Paleoclimatology. We are thankful for the constructive review comments from Roger Bales and an anonymous reviewer.

References

Allen, R. G., Walter, I. A., Elliott, R. L., Howell, T. A., Itenfisu, D., & Jensen, M. E. (Eds) (2005). *The ASCE standardized reference evapotranspiration equation*. Reston, VA: ASCE.

Anderson, E. A. (1976). *A point energy and mass balance model of a snow cover*, NOAA Tech. Rep. NWS 19, 150 pp. . Silver Spring, Md.: Natl. Oceanic and Atmos. Admin.

Anderson, R. M., Koren, V. I., & Reed, S. M. (2006). Using SSURGO data to improve Sacramento model a priori parameter estimates. *Journal of Hydrology*, *320*(1-2), 103–116. https://doi.org/10.1016/j.jhydrol.2005.07.020

Anderson, S., Moser, C. L., Tootle, G. A., Grissino-Mayer, H. D., Timilsena, J., & Piechote, T. (2012). Snowpack reconstructions incorporating climate in the Upper Green River Basin (Wyoming). *Tree-Ring Research*, *68*(2), 105–114. https://doi.org/10.3959/2011-8.1

Anderson, S.-R., Tootle, G., & Grissino-Mayer, H. D. (2012). Reconstruction of soil moisture for the Upper Colorado River basin using tree-ring chronologies. *Journal of the American Water Resources Association*, *48*, 1–10. https://doi.org/10.1111/j.1752-1688.2012.00651.x

Bales, C. R., Hopmans, J. W., O'Geen, A. T., Meadows, M., Hartsough, P. C., Kirchner, P., et al. (2011). Soil moisture response to snowmelt and rainfall in a Sierra Nevada mixed-conifer forest. *Vadose Zone Journal*, *10*, 786–799. https://doi.org/10.2136/vzj2011.0001

Bales, R. C., Goulden, M. L., Hunsaker, C. T., Conklin, M. H., Hartsoug, P. C., O'Geen, A. T., et al. (2018). Mechanisms controlling the impact of multi-year drought on mountain hydrology. *Scientific Reports*, *8*(1), 1–8. https://doi.org/10.1038/s41598-017-19007-0

Belmecheri, S., Babst, F., Wahl, E. R., Stahle, D. W., & Trouet, V. (2016). Multi-century evaluation of Sierra Nevada snowpack. *Nature Climate Change*, *6*(1), 2. https://doi.org/10.1038/nclimate2809

Bigelow, S. W., Papaik, M. J., Caum, C., & North, M. P. (2014). Faster growth in warmer winters for large trees in a Mediterranean-climate ecosystem. *Climatic Change*, *123*, 215–224. https://doi.org/10.1007/s10584-014-1060-0

Biondi, F., & Meko, D. M. (2019). Long-term hydroclimatic patterns in the Truckee-Carson Basin of the eastern Sierra Nevada, USA. *Water Resources Research*, *55*, 5559–5574. https://doi.org/10.1029/2019WR024735

Biondi, F., Perkins, D. L., Cayan, D. R., & Hughes, M. K. (1999). July temperature during the second millennium reconstructed from Idaho tree rings. *Geophysical Research Letters*, *26*(10), 1445–1448. https://doi.org/10.1029/1999gl900272

Brewer, P. (2014). Data management in dendroarchaeology using Tellervo. *Radiocarbon*, *56*(4), S79–S83. https://doi.org/10.2458/azu_rc.56.18320

Briffa, K. R., Jones, P. D., & Schweingruber, F. H. (1988). Summer temperature patterns over Europe: A reconstruction from 1750 AD based on maximum latewood density indices of conifers. *Quaternary Research*, *30*, 36–52. https://doi.org/10.1016/0033-5894(88)90086-5

Briffa, K. R., Jones, P. D., & Schweingruber, F. H. (1992). Tree-ring density reconstructions of summer temperature patterns across western North America since 1600. *Journal of Climate*, *5*, 735–754. https://doi.org/10.1175/1520-0442(1992)005<0735:trdros>2.0.co;2

Bunn, A. G., Salzer, M. W., Anchukaitis, K. J., Bruening, J. M., & Hughes, M. K. (2018). Spatiotemporal variability in the climate growth response of high elevation bristlecone pine in the White Mountains of California. *Geophysical Research Letters*, *45*, 13,312–13,321. https://doi.org/10.1029/2018GL080981

Burnash, R. J., Ferral, R. L., & McGuire, R. A. (1973). *A generalized streamflow simulation system conceptual modeling for digital computers*. Cooperatively developed by the U. S Department of Commerce National Weather Service and State of California Department of Water Resources.

Cook, E. R., & Holmes, R. L. (1999). *Program ARSTAN: Chronology development with statistical analysis (user's manual for program ARSTAN)*. Laboratory of Tree-Ring Research: University of Arizona. 18 pp.

Cook, E. R., & Kairiukstis, L. (1990). *Methods of dendrochronology: Applications in the environmental sciences*. Dordrecht, Netherlands: Springer Netherlands. ISBN: 0-7923-0586-8.

Cook, E. R., & Krusic, P. J. (2005). *A tree-ring standardization program based on detrending and autoregressive time series modeling, with interactive graphics*. Tree-Ring Laboratory, Lamont-Doherty Earth Observatory of Columbia University, Palisades: New York, USA.
Cook, E. R., Meko, D. M., Stahle, D. W., & Cleaveland, M. K. (1999). Drought reconstructions for the continental United States. *Journal of Climate*, *12*, 1145–1162. https://doi.org/10.1175/1520-0442(1999)012<1145:drftcu>2.0.co;2
Cook, E. R., Seager, R., Cane, M. A., & Stahle, D. W. (2007). North American drought: Reconstructions, causes, and consequences. *Earth-Science Reviews*, *81*, 93–134. https://doi.org/10.1016/j.earscirev.2006.12.002
Daly, C., Neilson, R. P., & Phillips, D. L. (1994). A statistical topographic model for mapping climatological precipitation over mountainous terrain. *Journal of Applied Meteorology*, *33*, 140–158. https://doi.org/10.1175/1520-0450(1994)033<0140:astmfm>2.0.co;2
Dolanc, C. R., Westfall, R. D., Safford, H. D., Thorne, J. H., & Schwartz, M. W. (2013). Growth–climate relationships for six subalpine tree species in a Mediterranean climate. *Canadian Journal of Forest Research*, *43*, 1114–1126. https://doi.org/10.1139/cjfr-2013-0196
Fritts, H. C. (1976). *Tree rings and climate*. London: Academic Press. 567 pp.
Fritts, H. C., Guiot, J., & Gordon, G. A. (1990). Verification. In E. R. Cook, & L. A. Kairiukstis (Eds.), *Methods of Dendrochronology: Applications in the Environmental Sciences*, (pp. 178–185). Dordrecht, Netherland: Kluwer Academic Publishers.
Georgakakos, K. P., & Smith, D. E. (2001). Soil moisture tendencies into the next century for the conterminous United States. *Journal of Geophysical Research-Atmospheres*, *106*(D21), 27,367–27,382. https://doi.org/10.1029/2001jd900125
Graham, N. E., & Hughes, M. K. (2007). Reconstructing the mediaeval low stands of Mono Lake, Sierra Nevada, California, USA. *The Holocene*, *17*, 1197–1210. https://doi.org/10.1177/0959683607085126
Graumlich, L. (1993). A 1,000-year record of temperature and precipitation in the Sierra Nevada. *Quaternary Research*, *39*, 249–255. https://doi.org/10.1006/qres.1993.1029
Graumlich, L. J., & Brubaker, L. B. (1986). Reconstruction of annual temperature (1590–1979) for Longmire, Washington, derived from tree rings. *Quaternary Research*, *25*(2), 223–234. https://doi.org/10.1016/0033-5894(86)90059-1
Graumlich, L. J., Pisaric, M. F. J., Waggoner, L. A., Littell, J. S., & King, J. C. (2003). Upper Yellowstone River flow and teleconnections with Pacific Basin climate variability during the past three centuries. *Climatic Change*, *59*(1-2), 245–262. https://doi.org/10.1007/978-94-015-1252-7_12
Gray, S. T., Jackson, S. T., & Betancourt, J. L. (2004). Tree-ring based reconstructions of interannual to decadal-scale precipitation variability for northeastern Utah. *Journal of the American Water Resources Association*, *40*, 947–960. https://doi.org/10.1111/j.1752-1688.2004.tb01058.x
Griffin, D., Woodhouse, C. A., Meko, D. M., Stahle, D. W., Faulstich, H. L., Carrillo, C., et al. (2013). North American monsoon precipitation reconstructed from tree-ring latewood. *Geophysical Research Letters*, *40*, 1–5. https://doi.org/10.1002/grl.50184
Grissino-Mayer, H. D. (2001). Evaluating crossdating accuracy: A manual tutorial for the computer program COFECHA. *Tree-Ring Research*, *57*, 205–221.
Gupta, H. V., Kling, H., Yilmaz, K. K., & Martinez, G. F. (2009). Decomposition of the mean squared error and NSE performance criteria: Implications for improving hydrological modelling. *Journal of Hydrology*, *377*(1-2), 80–91. https://doi.org/10.1016/j.jhydrol.2009.08.003 ISSN 0022-1694
Haan, C. T. (2002). *Statistical methods in hydrology*, (second ed.). Iowa, USA: Iowa State University Press. 496 pp.
Harpold, A. A. (2016). Diverging sensitivity of soil water stress to changing snowmelt timing in the western U.S. *Advances in Water Resources*, *92*, 116–129. https://doi.org/10.1016/j.advwatres.2016.03.017
Hastie, T., Tibshirani, R., & Friedman, J. (2013). *The elements of statistical learning: Data mining, inference and prediction*, (Second ed.). New York: Springer.
Holmes, R. L. (1983). Computer-assisted quality control in tree-ring dating and measurement. *Tree-Ring Bulletin*, *43*, 69–78.
Kelly, A. E., & Goulden, M. L. (2016). A montane Mediterranean climate supports year-round photosynthesis and high forest biomass. *Tree Physiology*, *36*(4), 459–468. https://doi.org/10.1093/treephys/tpv131
Kling, H., Fuchs, M., & Paulin, M. (2012). Runoff conditions in the upper Danube basin under an ensemble of climate change scenarios. *Journal of Hydrology*, *424-425*, 264–277. https://doi.org/10.1016/j.jhydrol.2012.01.011
Klos, P. Z., Goulden, M. L., Riebe, C. S., Tague, C. L., O'Geen, A. T., Flinchum, B. A., et al. (2018). Subsurface plant-accessible water in mountain ecosystems with a Mediterranean climate. *WIREs Water*, *5*. https://doi.org/10.1002/wat2.1269
Knoben, W. J. M., Freer, J. E., & Woods, R. A. (2019). Technical note: Inherent benchmark or not? Comparing Nash–Sutcliffe and Kling–Gupta efficiency scores. *Hydrology and Earth System Sciences*, *23*, 4323–4331. https://doi.org/10.5194/hess-23-4323-2019
Koren, V., Smith, M., & Duan, Q. (2003). Use of a priori parameter estimates in the derivation of spatially consistent parameter sets of rainfall-runoff models. In Q. Duan, S. Sorooshian, H. Gupta, H. Rosseau, & H. Turcotte (Eds.), *Calibration of Watershed Models Water Science and Applications* (Vol. 6, pp. 239–254). Washington, DC USA: AGU.
Littel, J. L., Peterson, D. L., & Tjolelker, M. (2008). Douglas-fir growth in mountain ecosystems: Water limits tree growth from stand to region. *Ecological Monographs*, *78*(3), 349–368. https://doi.org/10.1890/07-0712.1
Livneh, B., Rosenberg, E. A., Lin, C., Nijssen, B., Mishra, V., Andreadis, K. M., et al. (2013). A long-term hydrologically based dataset of land surface fluxes and states for the conterminous United States: Update and extensions. *Journal of Climate*, *26*, 9384–9392. https://doi.org/10.1175/jcli-d-12-00508.1
Lundquist, J. D., & Flint, A. L. (2006). Onset of snowmelt and streamflow in 2004 in the western United States: How shading may affect spring streamflow timing in a warmer world. *Journal of Hydrometeorology*, *7*(6), 1199–1217. https://doi.org/10.1175/jhm539.1 www.jstor.org/stable/24910940
Lundquist, J. D., Minder, J. R., Neiman, P. J., & Sukovich, E. S. (2010). Relationships between barrier jet heights, orographic precipitation gradients, and streamflow in the northern Sierra Nevada. *Journal of Hydrometeorology*, *11*, 1141–1156. https://doi.org/10.1175/2010JHM1264.1
Meko, D. M., & Baisan, C. H. (2001). Pilot study of latewood width of conifers as an indicator of variability ofsummer rainfall in the North American monsoon region. *International Journal of Climatology*, *21*, 697–708.
Meko, D. M., Stahle, D. W., Griffin, D., & Knight, T. A. (2011). Inferring precipitation-anomaly gradients from tree rings. *Quaternary International*, *235*, 89–100. https://doi.org/10.1016/j.quaint.2010.09.006
Meko, D. M., & Woodhouse, C. A. (2005). Tree-ring footprint of joint hydrologic drought in Sacramento and upper Colorado River basins, western USA. *Journal of Hydrology*, *308*, 196–213. https://doi.org/10.1016/j.jhydrol.2004.11.003
Michaelsen, J. (1987). Cross-validation in statistical climate forecast models. *Journal of Climate and Applied Meteorology*, *26*, 1589–1600. https://doi.org/10.1175/1520-0450(1987)026<1589:cviscf>2.0.co;2
Mote, P. W., Hamlet, A. F., Clark, M. P., & Lettenmaier, D. P. (2005). Declining mountain snowpack in western North America. *Bulletin of the American Meteorological Society*, *86*(1), 39–49. https://doi.org/10.1175/bams-86-1-39

Myers, R. H. (1990). *Classical and modern regression with applications*. Pacific Grove, California: Doxbury. 488 pp.
Nakawatase, J. M., & Peterson, D. L. (2006). Spatial variability in forest growth-climate relationships in the Olympic Mountains, Washington. *Canadian Journal of Forest Research*, *36*, 77–91. https://doi.org/10.1139/x05-224
Namias, J. (1978). Multiple causes of the North American abnormal winter 1976–77. *Monthly Weather Review*, *106*, 279–295. https://doi.org/10.1175/1520-0493(1978)106<0279:mcotna>2.0.co;2
National Weather Service River Forecast System (NWSRFS) User's Manual (1999). [Available from NOAA/National Weather Service, Office of Hydrology, 1325 East–West Hwy, Silver Spring, MD 20910.]
Pandey, G. R., Cayan, D. R., & Georgakakos, K. P. (1999). Precipitation structure in the Sierra Nevada of California during winter. *Journal of Geophysical Research*, *104*(D10), 12,019–12,030. https://doi.org/10.1029/1999JD900103
Pederson, G. T., Gray, S. T., Woodhouse, C. A., Betancourt, J. L., Fagre, D. B., Littell, J. S., et al. (2011). The unusual nature of recent snowpack declines in the North American Cordillera. *Science*, *333*(6040), 332–335. https://doi.org/10.1126/science.1201570
Peterson, D. W., & Peterson, D. L. (2001). Mountain hemlock growth responds to climatic variability at annual and decadal time scales. *Ecology*, *82*, 3330–3345. https://doi.org/10.2307/2680156
Royce, E. B., & Barbour, M. G. (2001). Mediterranean climate effects. II. Conifer growth phenology across a Sierra Nevada ecotone. *American Journal of Botany*, *88*(5), 919–932. https://doi.org/10.2307/2657045
Shamir, E., & Georgakakos, K. P. (2006). Distributed snow accumulation and ablation modeling in the American River Basin. *Advances in Water Resources*, *29*(4), 558–570. https://doi.org/10.1016/j.advwatres.2005.06.010
Shamir, E., & Georgakakos, K. P. (2007). Estimating snow depletion curves for American River basins using distributed snow modeling. *Journal of Hydrology*, *334*(1-2), 162–173. https://doi.org/10.1016/j.jhydrol.2006.10.007
Snyder, R. L., & Pruitt, W. O. (1985). Estimating reference evapotranspiration with hourly data. In *California Irrigation Management Information System Final Report* (Chapter VII, Vol. I.). Land, Air, and Water Resources Paper No. 10013-A. Davis, CA: University of California.
Sprague, A. (2009). Evaluating the effect of climate in a Sierra mixed conifer forest. *Berkeley Science Journal*, *13*, 44–53.
Stephenson, N. L. (1990). Climate control of vegetation distribution: The role of the water balance. *American Naturalist*, *135*, 649–670. https://doi.org/10.1086/285067
Stephenson, N. L. (1998). Actual evapotranspiration and deficit: biologically meaningful correlates of vegetation distribution across spatial scales. *Journal of Biogeography*, *25*, 855–887. https://doi.org/10.1046/j.1365-2699.1998.00233.x
Stockton, C. W., & Meko, D. M. (1975). A long-term history of drought occurrence in western United States as inferred from tree rings. *Weatherwise*, *28*(6), 245–249. https://doi.org/10.1080/00431672.1975.9931775
Stokes, M. A., & Smiley, T. L. (1996). *An introduction to tree-ring dating*. Tucson: University of Arizona Press. (originally published 1968 University of Chicago Press), 73 pp.
Timilsena, J., & Piechota, T. (2008). Regionalization and reconstruction of snow water equivalent in the upper Colorado River basin. *Journal of Hydrology*, *352*, 94–106. https://doi.org/10.1016/j.jhydrol.2007.12.024
Touchan, R., Woodhouse, C. A., Meko, D. M., & Allen, C. (2011). Millennial precipitation reconstruction for the Jemez Mountains, New Mexico, reveals changing drought signal. *International Journal of Climatology*, *31*(6), 896–906. https://doi.org/10.1002/joc.2117
Tunnicliff, B. M. (1975). *The historical potential of snowfall as a water resources in Arizona, Master's thesis*. Tucson: University of Arizona, School of Renewable Natural Resources. 137 pp.
Vaganov, E. A., Hughes, M. K., Kirdyanov, A. V., Schweingruber, F. H., & Silkin, P. P. (1999). Influence of snowfall and melt timing on tree growth in subarctic Eurasia. *Nature*, *400*, 149–151. https://doi.org/10.1038/22087
Vaganov, E. A., Hughes, M. K., & Shashkin, A. V. (2006). *Growth dynamics of conifer tree rings, images of past and future environments*. Berlin Heidelberg New York: Springer. 351 pp.
Wang, J., & Georgakakos, K. P. (2005). Validation and sensitivities of dynamic precipitation simulation for winter events over the Folsom Lake watershed: 1964–1999. *Monthly Weather Review*, *133*, 3–19. https://doi.org/10.1175/mwr-2814.1
Woodhouse, C. A. (2003). A 431-year reconstruction of western Colorado snowpack from tree rings. *Journal of Climate*, *16*, 1551–1561. https://doi.org/10.1175/1520-0442(2003)016<1551:ayrowc>2.0.co;2
Woodhouse, C. A., Gray, S. T., & Meko, D. M. (2006). Updated streamflow reconstructions for the Upper Colorado River Basin. *Water Resources Research*, *42*(W05415). https://doi.org/10.1029/2005wr004455
Yeh, H.-Y., & Wensel, L. C. (2000). The relationship between tree diameter growth and climate for coniferous species in Northern California. *Canadian Journal of Forest Research*, *30*, 1463–1471. https://doi.org/10.1139/x00-074
Yin, Z. Y., Shao, X., Qin, N., & Liang, E. (2008). Reconstruction of a 1,436-year soil moisture and vegetation moisture use history based on tree-ring widths from Qilian Junipers in northeastern Qaidam basin, northwestern China. *International Journal of Climatology*, *28*, 37–53. https://doi.org/10.1002/joc.1515